THE JOURNAL OF BIOLOGICAL CHEMISTRY VOL. 286, NO. 48, pp. 41776–41785, December 2, 2011

Phosphorylation of a PDZ Domain Extension Modulates Binding Affinity and Interdomain Interactions in Postsynaptic Density-95 (PSD-95) Protein, a Membrane-associated Guanylate Kinase (MAGUK)*[S]

Received for publication, June 24, 2011, and in revised form, September 9, 2011 Published, JBC Papers in Press, September 30, 2011, DOI 10.1074/jbc.M111.272583

Jun Zhang[‡], Chad M. Petit[‡], David S. King[§], and Andrew L. Lee[‡¶1]

From the [‡]Department of Biochemistry and Biophysics, School of Medicine and [¶]Division of Chemical Biology and Medicinal Chemistry, Eshelman School of Pharmacy, University of North Carolina, Chapel Hill, North Carolina 27599 and [§]Howard Hughes Medical Institute Mass Spectrometry Laboratory and Department of Molecular and Cell Biology, University of California, Berkeley, California 94720

Postsynaptic density-95 is a multidomain scaffolding protein that recruits glutamate receptors to postsynaptic sites and facilitates signal processing and connection to the cytoskeleton. It is the leading member of the membrane-associated guanylate kinase family of proteins, which are defined by the PSD-95/Discs large/ZO-1 (PDZ)-Src homology 3 (SH3)-guanylate kinase domain sequence. We used NMR to show that phosphorylation of conserved tyrosine 397, which occurs *in vivo* and is located in an atypical helical extension (α3), initiates a rapid equilibrium of docked and undocked conformations. Undocking reduced ligand binding affinity allosterically and weakened the interaction of PDZ3 with SH3 even though these domains are separated by a ~25-residue linker. Additional phosphorylation at two linker sites further disrupted the interaction, implicating α3 and the linker in tuning interdomain communication. These experiments revealed a novel mode of regulation by a detachable PDZ element and offer a first glimpse at the dynamic interaction of PDZ and SH3-guanylate kinase domains in membrane-associated guanylate kinases.

Phosphorylation is one of the most common modifications made to proteins. Depending on the protein substrate, it can regulate the gain or loss of activity through a variety of mechanisms. Most mechanisms studied to date appear to work via a change in steric geometry at the active site or a global conformational change in the protein (1–3), although a few recent examples indicate modulation of protein dynamics that can yield a graded response (4, 5). In some cases, phosphorylation simply provides a protein-protein recognition site (6). Overall, the extent of structural characterization of phosphorylation mechanisms is limited given the ubiquity of this post-translational signaling mechanism and the large diversity of effects observed upon phosphorylation. A greater understanding of how phosphorylation(s) modulates protein activity is essential for a mechanistic understanding of signal transduction.

Many phosphorylated proteins are multidomain, modular proteins (2–4). One class of such proteins that shape signal transduction is the scaffolding proteins, which are frequently phosphorylated (7). Membrane-associated guanylate kinase (MAGUK)[2] family proteins are multidomain scaffolding proteins that play roles in ion channel clustering, intracellular trafficking, signal transduction, and cell-cell adhesion (8–10). Malfunction of MAGUKs is associated with central nervous system disorders (11). The defining MAGUK signature is the PDZ-SH3-guanylate kinase "supradomain" architecture. The best known MAGUK protein is postsynaptic density-95 (PSD-95), which is found on the cytoplasmic side of postsynaptic terminals. PSD-95 is a non-catalytic scaffolding protein that clusters glutamate receptors and assembles macromolecular complexes for signal integration in the postsynapse at excitatory neurons (8, 12). It consists of three PDZ domains, an SH3 domain, and a non-catalytic guanylate kinase (GK) domain (see Fig. 1*A*). PDZ domains are ~90-residue, globular, protein interaction domains that have a conserved fold comprised of two α-helices and six β-strands. The function of PDZs is typically to bind the C-terminal 4–5 residues of target proteins, which bind in a groove between α2 and β2 of the PDZ. PDZ domains are often found in tandem copies and are common to proteins that function as scaffolds for assembling signaling complexes or trafficking components at cell-cell junctions. In PSD-95, the three PDZ domains bind many proteins ranging from NMDA and adrenergic receptors to neuronal nitric-oxide synthase, Pyk2, synaptic Ras GTPase activating protein, and microtubule assemblies (13). Structural work has been carried out on individual PDZs of PSD-95 (14, 15) as well as the SH3-GK module (16, 17). However, little is known about how MAGUK PDZ domains associate/function with the SH3-GK module. A role for PDZs beyond their normal C-terminal ligand binding function has

* This work was supported by National Science Foundation Grant MCB-0344354 (to A. L. L.) and bridge funding provided by the University of North Carolina and the Eshelman School of Pharmacy.

[S] The on-line version of this article (available at http://www.jbc.org) contains supplemental Table S1 and Figs. S1–S5.

[1] To whom correspondence should be addressed: Division of Chemical Biology and Medicinal Chemistry, Eshelman School of Pharmacy, University of North Carolina, Beard Hall, CB 7568, Chapel Hill, NC 27599-7568. Tel.: 919-966-7821; Fax: 919-843-5130; E-mail: drewlee@unc.edu.

[2] The abbreviations used are: MAGUK, membrane-associated guanylate kinase; S^2, order parameter characterizing amplitude of amide bond; PDZ, PSD-95/Discs large/Zo-1; PSD, postsynaptic density; SH3, Src homology 3; GK, guanylate kinase; SEA, solvent-exposed amide; HSQC, heteronuclear single quantum correlation; CSP, chemical shift perturbation; ITC, isothermal titration calorimetry.

emerged from examples in which intermolecular (or interdomain) contacts occur on novel PDZ interfaces (18, 19) or binding is regulated allosterically (18, 20–23).

Previous work suggests that the third PDZ domain (PDZ3) in PSD-95 family proteins regulates activity at SH3-GK, indicating that this PDZ domain may have an additional regulatory function on top of its C-terminal binding function. MAP1a binds to the GK domain of PSD-95; however, this interaction is weakened by the presence of PDZ3 (and abolished by the presence of all three PDZ domains) and restored by PDZ-binding peptides such as adenomatous polyposis coli, NR2B, and cysteine-rich PDZ-binding protein (24). Interdomain interactions were also characterized in the *Drosophila* homologue of PSD-95, Dlg-1, in which the domain interaction between PDZ3 and SH3 was regulated by PDZ3-binding peptides (25). The region linking PDZ3 and SH3 is vital to the interdomain communication between these two domains: replacement of the conserved linker region with flexible Gly-Ser repeats disrupts the influence that PDZ3 has on the binding of SH3 to its interaction partner, GukHolder (25). Thus, a major question regarding MAGUKs is what is the role of the PDZ domain preceding SH3-GK and how might it participate in intramolecular, interdomain interactions?

Interestingly, PSD-95 is known to be phosphorylated at up to ~12 sites with several of these sites occurring at linker positions in between structured domains as well as one in a C-terminal helical extension to PDZ3 (see Fig. 1*A*). To date, phosphorylation has received modest attention as a means of regulating PDZ domain function in general. One exception is the PDZ protein NHERF1 for which phosphorylation has been shown to regulate PDZ-mediated autoinhibition (26). Recently, we showed that folding of a C-terminal extension to PDZ3 into an α-helix (third α-helix (α3)) increases binding affinity to PDZ3 ligand via an allosteric mechanism rooted in changes in picosecond-nanosecond side-chain dynamics (21). The α3 helix is not part of the conserved PDZ fold and hence appeared as an unusual auxiliary element whose function had been unclear. Within the α3 helix, Tyr-397 has been shown to be phosphorylated (27), which in principle could either increase or decrease α3 interactions with the PDZ core. In addition to Tyr-397, the nearby residues Ser-415 and Ser-418 can also be phosphorylated (28, 29). This dense collection of phosphorylation sites suggests that this region (C-terminal extension of PDZ3 and the PDZ3-SH3 linker) is a hot spot for MAGUK regulation. Interestingly, structured "extensions" to PDZ domains are now being discovered in more PDZ domains (30).

To probe the role of PDZ3 in the PSD-95 MAGUK and its transition into the linker and SH3 domain, we chose to study by NMR the effect of phosphorylation at three sites in the C-terminal region of PDZ3 and how such phosphorylations modulate PDZ3 structure, function, and its interaction with SH3-GK. A construct of PDZ3 spanning residues 304–402 was phosphorylated at Tyr-397 (p^{397}-PDZ3) and characterized for structural effects. A combination of chemical shift analysis, hydrogen exchange, ^{15}N relaxation, and isothermal titration calorimetry showed that phosphorylation induces a fast equilibrium between a docked conformation in which α3 is packed against the PDZ core and a conformational state in which α3 is undocked that has reduced affinity for PDZ3 ligands. The latter state was previously identified via truncation of α3 and shown to alter PDZ3 ligand binding affinity through a novel allosteric mechanism driven by side-chain dynamics (21). The findings here support this mechanism by showing that the dynamic allostery can be triggered by a biologically relevant modification and is likely to be utilized in a cellular context. In a second construct of PSD-95 that includes PDZ3-linker-SH3, phosphorylation at all three sites (397, 415, and 418) was shown to increase the mobility of PDZ3 relative to SH3. These studies provide insight into how phosphorylation affects structure and dynamics of an intrinsically flexible, multidomain system. They also show for the first time that the association of PDZ3 with the SH3 domain in PSD-95 is weakened by multiple phosphorylations.

EXPERIMENTAL PROCEDURES

Protein Expression and Purification—PDZ3 (residues 304–402), Y397E-PDZ3, and PDZ3-SH3 tandem (residues 304–532) from rat PSD-95 were subcloned into the pET21a vector with a tobacco etch virus-cleavable N-terminal histidine tag. The PDZ3-SH3 tandem was stabilized by adding the sequence SGSGSG**PYIWVPAREERL** to its C terminus (16) where bold residues are from residues 713 to 724, which form the F-strand of the SH3 domain. Y397E-PDZ3, PDZ3-SH3 single mutant (Y937E-PDZ3-SH3), and triple mutant (Y397E/S415E/S418E) were made by multiple site mutagenesis PCR (31). Transformed *Escherichia coli* BL21(DE3) cells were grown at 37 °C in LB medium or minimal medium containing appropriate isotopes. When cell density reached an A_{600} of 0.6, isopropyl 1-thio-β-D-galactopyranoside was added to a final concentration of 1 mM, and the cells were grown for another 16 h at 22 °C. The cells were harvested by centrifugation and stored at −80 °C until use.

To purify all proteins in this study, the cell pellets were resuspended in 50 mM Tris-HCl, pH 8.0, 200 mM NaCl, 0.1% Triton X-100, 25 mM imidazole, and 1 mM lysozyme. The resuspended cells were frozen and thawed for three cycles, and sonication was applied. The centrifuged cell lysate was loaded to a nickel affinity column and eluted with 500 mM imidazole. The fractions containing target proteins were pooled and subjected to overnight tobacco etch virus cleavage at 4 °C. A 100% cleavage was achieved as suggested by SDS-PAGE. Cleaved samples were further purified by Source Q ion exchange chromatography followed by a G50 size exclusion column equilibrated in a buffer containing 22 mM $NaPO_4$, pH 6.8, 55 mM NaCl, and 1.1 mM EDTA. p^{397}-PDZ3 was separated from PDZ3 using Source Q resin with a 260-ml linear gradient from 0 to 500 mM NaCl in 20 mM Tris-HCl, pH 7.0 (Fig. 2*A*). The identity and purity of the protein were verified by mass spectrometry and SDS-PAGE. Protein concentrations were determined by UV absorbance with extinction coefficients calculated by the ProtParam tool. Phosphorylation changes the UV absorbance profile of tyrosine with an extinction coefficient of 593 M^{-1} cm^{-1} at 268 nm (32). Taking the other unphosphorylated tyrosine (Tyr-392; ϵ_{268} = 1114 M^{-1} cm^{-1}) into account, the concentration of p^{397}-PDZ3 was determined using an extinction coefficient of 1707 M^{-1} cm^{-1} at 268 nm.

PDZ3-SH3 single and triple mutants were purified using the aforementioned protocol with modification at the size exclusion chromatography step where elution buffer contained 50 mM Tris-HCl, pH 7.5, 200 mM NaCl, and 1 mM DTT. The plasmid encoding c-Src kinase was a gift from John Kuriyan (University of California, Berkeley) and Sharon Campbell (University of North Carolina at Chapel Hill). The c-Src kinase domain was purified as described (33).

Peptide Synthesis—A 7-mer CRIPT peptide (Ac-NYKQTSV-COOH) was synthesized and purified as reported (21). The identity and purity of the peptide were verified by mass spectrometry. The peptide concentration was determined using UV absorbance with an extinction coefficient of 1490 M^{-1} cm^{-1}.

Isothermal Titration Calorimetry Experiments—ITC experiments were carried out on a MicroCal VP-ITC microcalorimeter and repeated twice to estimate error. ITC measurements of PDZ3, p^{397}-PDZ3, and Y397E-PDZ3 were performed by titrating 1 mM CRIPT peptide into 0.1 mM protein. In total, 280 μl of CRIPT peptide was titrated into 1.4 ml of protein solution by 40 steps with a 3-min interval between injections. The dilution effect was estimated by performing the same titration procedure without protein. Both the peptide and proteins were dissolved in the same buffer containing 20 mM $NaPO_4$, pH 6.8, 50 mM NaCl, and 1 mM EDTA. Data were integrated and analyzed using Origin version 5.0 (MicroCal). K_d, ΔH, ΔS, and N were fitted with a single binding site model. For PDZ3, p^{397}-PDZ3, and Y397E-PDZ3 titrations, c values were 27.8, 7.2, and 12.6, respectively.

NMR Assignments and Relaxation Experiments—PDZ3, p^{397}-PDZ3, and Y397E-PDZ3 NMR samples were dissolved in 20 mM $NaPO_4$, pH 6.8, 50 mM NaCl, 1 mM EDTA, and 10% D_2O at a protein concentration of 1 mM. NMR assignment data were acquired on a Varian Inova 500-MHz magnet equipped with a room temperature $^1H/^{15}N/^{13}C$ probe and z axis pulsed field gradients. Backbone resonance assignments for p^{397}-PDZ3 and Y397E-PDZ3 were obtained using three-dimensional HNCACB and CBCA(CO)NH experiments (34).

For characterization of backbone dynamics of p^{397}-PDZ3, ^{15}N T_1, T_2, and $\{^1H\}$-^{15}N NOE data (supplemental Fig. S1) were collected at 500 MHz at a protein concentration of 1 mM. Data were acquired and analyzed as reported elsewhere (21, 35) using in-house programs. Briefly, T_1, T_2, and $\{^1H\}$-^{15}N NOE data from "rigid" residues were initially fit to obtain the overall correlation time of the protein, which was determined to be 6.8 ns. As with unphosphorylated PDZ3, anisotropic models of tumbling were not required (21). Models were then selected for individual residues (supplemental Table S1) to fit the Lipari-Szabo dynamics parameters (S^2, τ_e, etc.).

^{15}N T_2 relaxation data for wild-type PDZ3-SH3 and Y397E-PDZ3-SH3 and Y397E/S415E/S418E-PDZ3-SH3 mutants were acquired at a protein concentration of 0.5 mM. Data were collected as described (21) on a Varian Inova 500-MHz system equipped with a $^1H/^{15}N/^{13}C$ cryogenically cooled probe with z axis pulsed field gradients. Wild-type and mutant PDZ3-SH3 constructs were dissolved in a buffer containing 50 mM Tris-HCl, pH 7.5, 200 mM NaCl, 10% D_2O, and 1 mM DTT. All NMR spectra were processed by NMRPipe and analyzed by NMRViewJ.

Solvent-exposed Amide (SEA)-HSQC Experiments—Solvent-exposed amide HSQC spectra were collected at 500 MHz using a $^1H/^{15}N/^{13}C$ probe and z axis pulsed field gradients at 298 K. The original SEA-HSQC pulse sequence was developed by Lin *et al.* (36) using a clean chemical exchange-phase modulated-PM mixing scheme. In this study, a Biopack version of the SEA-HSQC pulse sequence was used. The intertransient delay was set to 1.5 s, and the mixing time was 0.1 s. The spectra of PDZ3 and p^{397}-PDZ3 were collected at a protein concentration of 1 mM with 16 transients. NMR intensity is a function of several factors such as protein concentration, nuclear relaxation time, solution conductivity, and protein tumbling time. Of these factors, protein tumbling time is significantly influenced by phosphorylation (see "Results"). This necessitates a method to scale the SEA-HSQC intensities of PDZ3 and p^{397}-PDZ3 to allow direct comparison. The scaling procedure used the residues that are not affected by phosphorylation, *i.e.* those residues that experience slight or nearly no chemical shift perturbation as shown in Fig. 2*A*. The SEA-HSQC peak intensities of p^{397}-PDZ3 for these residues were scaled to match those of PDZ3.

RESULTS

Phosphorylation of Tyr-397 and Purification of Phosphorylated PDZ3—From the crystal structure of PDZ3 (14), the side chain of Tyr-397 is partially buried between α3 and the core domain of PDZ3 (Fig. 1*B*). This tyrosine residue is phosphorylated in mouse brain (27), although it is unknown which kinase *in vivo* is responsible for its phosphorylation. Tyr-397, located at the linker between PDZ3 and SH3, is highly conserved throughout MAGUK proteins of various organisms (Fig. 1*A*). Using the ExPASy Proteomics Server, we analyzed the first 100 homologue sequences of PSD-95, which belong to different organisms, different subfamilies, and different splicing forms. Only one conserved mutation (Tyr to Phe) was found. The high conservation of Tyr-397 implies its significance within the MAGUK family. Members of the Src family are known to interact with PSD-95 (37). Using the Group-based Prediction System (38), Src kinase was predicted to be capable of phosphorylating Tyr-397. Treatment of ^{15}N-labeled PDZ3 with c-Src resulted in a new set of resonances in the HSQC spectrum of PDZ3. The relative peak intensities suggested that only 10% of PDZ3 was phosphorylated. The reaction went further to completion after removing ADP by dialysis and adding fresh ATP, which was repeated four times. This yielded ~40% putative p^{397}-PDZ3.

Ion exchange chromatography was used to purify p^{397}-PDZ3 based on the additional negative charge introduced by phosphorylation. The elution profile displayed five discrete species, three of which tested positive for protein (Fig. 2*A*). The first peak was confirmed to be PDZ3 from HSQC, and the third peak was confirmed to be pure phospho-PDZ3. An overlay of HSQC spectra of PDZ3 and putative p^{397}-PDZ3 shows peaks shifting in regions of PDZ3 consistent with modification at Tyr-397 (Fig. 2*B*). The identity of the third peak was also analyzed by mass spectrometry (supplemental Fig. S2). Although the electrospray ionization ion trap mass spectrum indicated the correct mass for a singly phosphorylated species (supplemental Fig. S2A), MS-MS MALDI-TOF results suggested that the

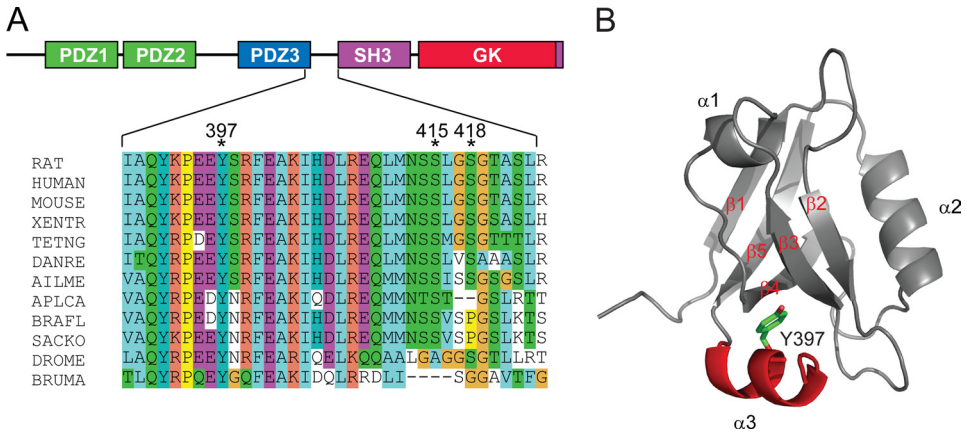

FIGURE 1. **Domain architecture of PSD-95 and crystal structure of PDZ3.** *A*, the five domains of PSD-95 are shown, and the sequences of the α3 region and PDZ3-SH3 linker in MAGUK family from different organisms are aligned. The conserved tyrosine (Tyr-397) and two serine phosphorylation sites (Ser-415 and Ser-418) are denoted by "*." The alignment was done using ClustalX 2.0.12. *RAT*, *Rattus norvegicus*; *MOUSE*, *Mus musculus*; *XENTR*, *Xenopus* (*Silurana*) *tropicalis*; *TETNG*, *Tetraodon nigroviridis*; *DANRE*, *Danio rerio*; *AILME*, *Ailuropoda melanoleuca*; *APLCA*, *Aplysia californica*; *BRAFL*, *Branchiostoma floridae* (Florida lancelet) (amphioxus); *SACKO*, *Saccoglossus kowalevskii* (acorn worm); *DROME*, *Drosophila melanogaster*; *BRUMA*, *Brugia malayi* (filarial nematode worm). *B*, the crystal structure of PDZ3 (Protein Data Bank code 1BFE) is shown in the schematic. Tyr-397 is shown in *sticks*. The α3 is shown in *red*..

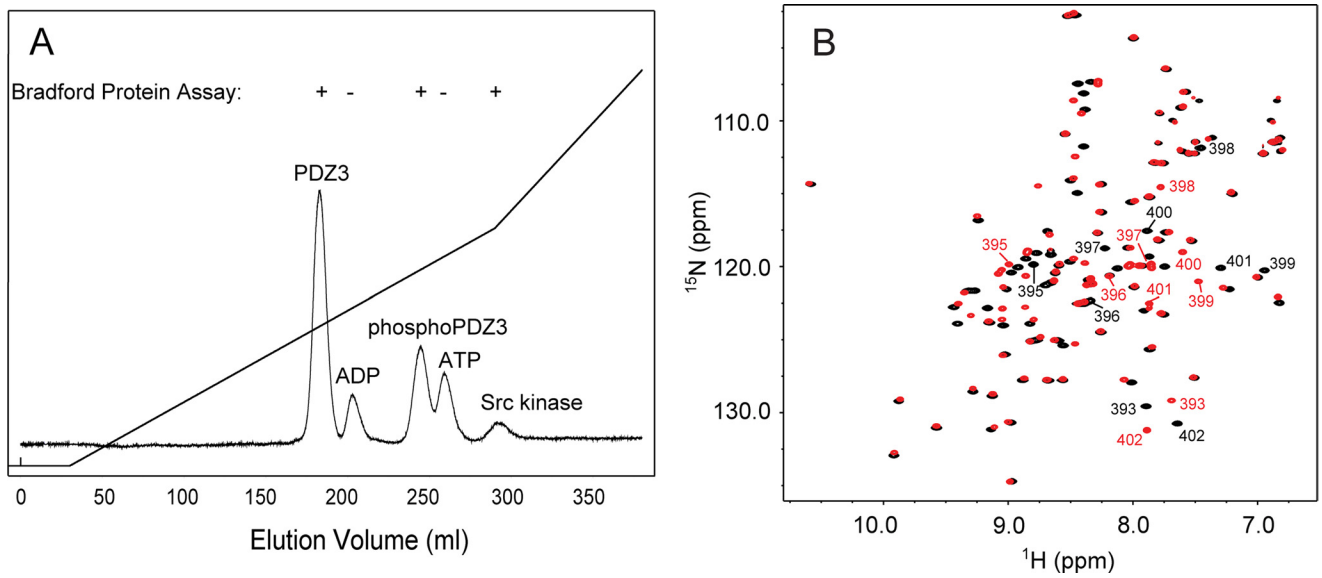

FIGURE 2. **Purification of p^{397}-PDZ3.** *A*, ion exchange chromatography elution profile of p^{397}-PDZ3 purification monitored by UV absorbance at 280 nm. The NaCl elution gradient is shown as *straight lines*. *B*, ^{15}N HSQC of p^{397}-PDZ3 (*red*) and PDZ3(304–402) (*black*). The resonances of residues at α3 are indicated.

dominant species of the third peak was p^{397}-PDZ3, although small amounts of p^{392}-PDZ3 (<10%) could not be not ruled out (supplemental Fig. S2B). A species other than p^{397}-PDZ3 was not found in ^{1}H-^{15}N HSQC, HNCO, HNCACB, or CBCA-(CO)NH spectra. Based on this, the following NMR-based observations were interpreted to arise solely from p^{397}-PDZ3. The above procedure was used to obtain milligram quantities of p^{397}-PDZ3 for further biophysical characterization.

Phosphorylation-induced Undocking of α3 Lowers Affinity for CRIPT Ligand—To determine the effect of phosphorylation at Tyr-397 on PDZ3 structure, the backbone chemical shifts of p^{397}-PDZ3 were assigned and compared with unphosphorylated PDZ3 (Fig. 3*A*). These chemical shift perturbations (CSPs) were then mapped onto the structure of PDZ3 (Fig. 3*B*). Phosphorylation resulted in CSPs radiating out from Tyr-397 to include all of α3 and its surrounding regions. Although the perturbation pattern is consistent with the general site of phosphorylation, the extent and specific nature of any structural change accompanying phosphorylation is more difficult to assess strictly from CSPs.

In unphosphorylated PDZ3, the side chain of Tyr-397 packs into side chains of the β2 strand, the β3 strand, and the α1-β4 loop of the PDZ core. These hydrophobic interactions help to define how α3 packs against the PDZ core (Fig. 3*B*). One possible consequence of phosphorylation is therefore destabilization/unfolding of α3 because the phosphate group might occlude proper packing of α3. In this sense, phosphorylation of Tyr-397 would effectively convert PDZ3 into a C-terminally truncated form, much like PDZ(303–395) characterized previously and referred to as Δ7ct (21). To test this idea, we compared [^{1}H, ^{15}N] amide chemical shifts of PDZ3, p^{397}-PDZ3, and Δ7ct by superimposing HSQCs of the three proteins. Nearly all residues experiencing significant CSPs in p^{397}-PDZ3 (Fig. 3) display a linear trend of HSQC peaks in the order PDZ3, p^{397}-PDZ3, and Δ7ct (Fig. 4*A*). To quantitatively demonstrate linearity of these three sets of resonances, correlation values

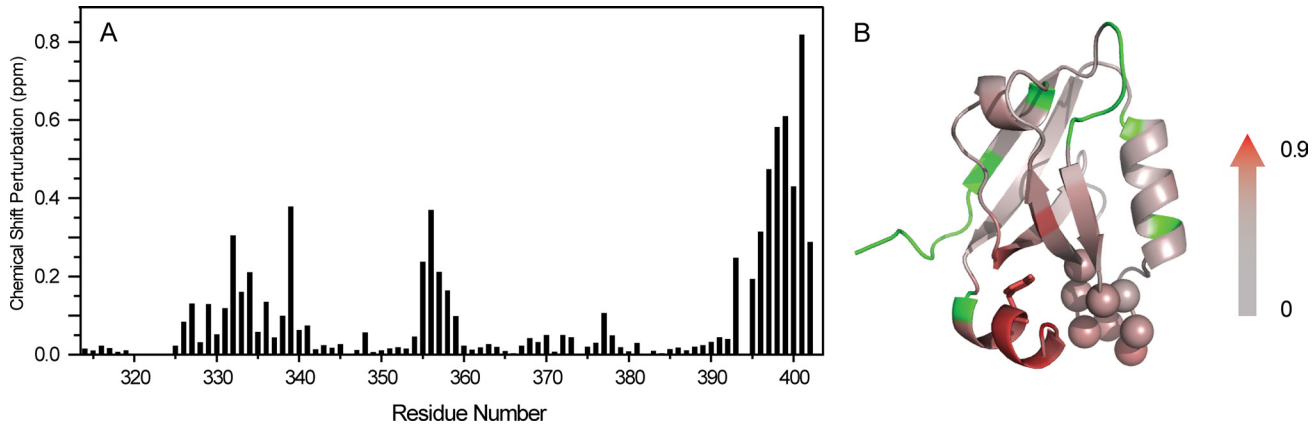

FIGURE 3. **CSP of Tyr-397 phosphorylation.** The ^{15}N HSQCs of PDZ3 and p^{397}-PDZ3 were compared, and vector chemical shift changes of ^{1}H and ^{15}N are plotted *versus* residue number (*A*) and onto the crystal structure of PDZ3 (*B*) using a color scale. The vector chemical shift perturbations were calculated as $|\Delta\delta^{1}H| + 0.1 \times |\Delta\delta^{15}N|$. Tyr-397 is rendered in *sticks*, residues 329–336 (includes the β2-β3 loop) are rendered in *spheres*, and residues without CSP data are colored *green*. The graphic was prepared based on the structure of unliganded PDZ3 (Protein Data Bank code 1BFE).

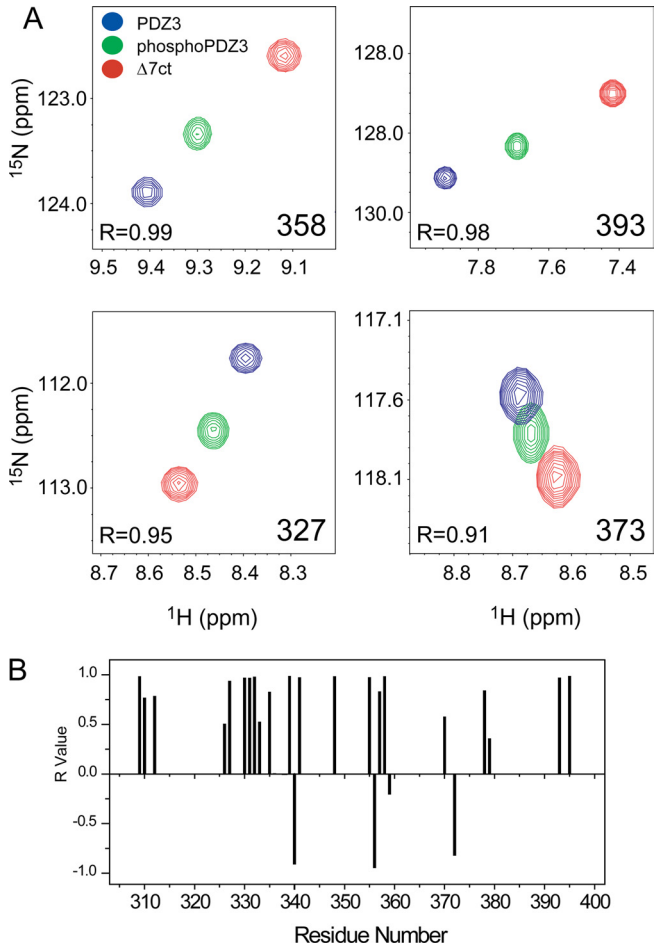

FIGURE 4. **Linear chemical shift pattern of PDZ3, p^{397}-PDZ3, and Δ7ct ^{15}N HSQC peaks.** *A*, four representative residues were selected to show the HSQC resonance pattern of PDZ3, p397-PDZ3, and Δ7ct. HSQC peaks of p^{397}-PDZ3 (*green*) fall onto the line defined by PDZ3 (*blue*) and Δ7ct (*red*) resonances. The adjusted correlation value (*R* value) for each example residue is given in each panel. *B*, adjusted correlation values (*R* values) of the resonances with significant chemical shift changes upon phosphorylation. Only the residues with CSP >0.05 ppm were analyzed.

(adjusted *R* values) of linear fitting were calculated and plotted (Fig. 4*B*). Most *R* values are around 1, indicating high linearity for many residues. Because chemical shifts are highly nonlinear with respect to positioning of structural elements, such extensive linearity cannot be reasonably explained as accidental. Rather, the simplest explanation is that the peak positions of p^{397}-PDZ3 are averaged due to fast exchange between two conformations: one in which α3 is packed as in native PDZ3 and one in which α3 is undocked and makes no contributions to chemical shifts in PDZ core residues. Thus, p^{397}-PDZ3 exists as an equilibrium of two dynamically exchanging states represented by PDZ3 and Δ7ct, respectively. Preliminary ^{15}N Carr-Purcell-Meiboom-Gill relaxation dispersion experiments (39) on p^{397}-PDZ3 did not detect this exchange; and thus, we conclude that exchange takes place on the microsecond or possibly even nanosecond timescale. Because p^{397}-PDZ3 peaks occurred on average approximately half-way between unphosphorylated PDZ3 and Δ7ct peaks, the fraction of undocked α3 was estimated to be ~50%.

It was shown previously that truncation of α3 decreases binding affinity of PDZ3 with CRIPT peptide by 21-fold (21). If p^{397}-PDZ3 is indeed a mixture of PDZ3- and Δ7ct-like states, an intermediate binding affinity to CRIPT peptide should be observed. To test this, we performed ITC experiments to measure the binding affinity of p^{397}-PDZ3 to CRIPT C-terminal peptide. The binding affinity of p^{397}-PDZ3 was found to be ~4 times weaker than PDZ3, falling in between PDZ3 and Δ7ct (Table 1). Importantly, this change in K_d due to phosphorylation is mainly attributed to entropy, which is the same signature observed for Δ7ct (21).

Phosphorylation of Tyr-397 Increases Disorder in α3—Phosphorylation of Tyr-397 disrupts the packing of α3 with the core domain of PDZ3 as described above. However, it is unknown how phosphorylation affects the local structure of α3. Does α3 still maintain its secondary structure when α3 is undocked from PDZ3? To answer this question, we analyzed ^{13}C chemical shifts, amide exchange rates, and ^{15}N backbone relaxation in phosphorylated and unphosphorylated PDZ3.

The $^{13}C^{\alpha}$ chemical shift relative to random coil values is a sensitive indicator of secondary structure (40). These relative chemical shift values for unphosphorylated PDZ3 and p^{397}-PDZ3 are shown for the C-terminal residues that include $\beta5^{385-392}$ and $\alpha3^{394-398}$ (Fig. 5). Phosphorylation clearly

TABLE 1
ITC binding parameters for PDZ3 and p^{397}-PDZ3
CRIPT peptide (NYKQTSV) was titrated in, and each experiment was repeated twice. The K_d between Δ7ct and CRIPT is 81 μM.

Binding parameters	PDZ3	p^{397}-PDZ3
Stoichiometry	0.98 ± 0.03	0.99 ± 0.02
K_d (μM)	3.60 ± 0.28	14.00 ± 0.47
ΔH (kcal/mol)	−8.57 ± 0.31	−8.80 ± 0.29
$-T\Delta S$ (kcal/mol)	−1.16 ± 0.26	−2.18 ± 0.31

diminished helicity in α3 as determined from the $^{13}C^{\alpha}$ chemical shift, whereas it had no effect on β5 structure.

Amide proton exchange reports on solvent accessibility and the stability of secondary structure. We measured these exchange rates using the SEA-HSQC experiment. This approach was used because the amides in the α3 region exchange rapidly (data not shown). In a SEA-HSQC spectrum, the intensity of an amide resonance is proportional to the extent to which it is solvent-exposed (36). As shown in supplemental Fig. S3A, only surface-exposed residues of PDZ3 are observed in the spectrum. The undocking of α3 is expected to increase solvent exposure, which should be evident from SEA-HSQC intensity changes. However, it is not appropriate to directly compare SEA-HSQC intensities of PDZ3 and phospho-PDZ3 samples as intensities are differentially affected by protein concentration and tumbling times. Therefore, intensities were normalized (see "Experimental Procedures") to facilitate direct comparison. SEA-HSQC peak intensities of PDZ3 and p^{397}-PDZ3 are plotted against one another in supplemental Fig. S3B. A good correlation of these peak intensities is obtained as indicated by an R value of 0.98, and a slope of 0.74 (for p^{397}-PDZ3 relative to PDZ3) was observed. As expected, α3 and its docking region displayed increased solvent exchange (supplemental Fig. S3, C and D), whereas other regions have few significant changes in solvent accessibility.

To directly determine the degree of flexibility in p^{397}-PDZ3, we used ^{15}N backbone relaxation coupled with model-free analysis (41) to yield an order parameter, S^2, for each residue. The most significant change in S^2 upon phosphorylation was in the α3 region, which showed decreases of 0.1–0.3 (Fig. 6). For residues in α3 with significant helicity (394–400), the average decrease in S^2, however, is only 0.10. Given that the undocked fraction was ~50% and that the docked state showed average S^2 values of ~0.85, this suggests that the undocked fraction yields on average S^2 values of ~0.65 for residues 394–400; this is much higher than expected for a fully unfolded C-terminal tail. Thus, it is more likely that upon undocking these "α3" residues redistribute some of their helical character into a mixture of extended and random coil-like states with the latter contributing most significantly to a decrease in S^2. This would allow for relatively high S^2 values and the observed $^{13}C^{\alpha}$ chemical shifts because extended backbone conformations would help to reduce the downfield shifts from random coil values (Fig. 5). In addition to S^2 effects at the C terminus, a slight overall decrease in S^2 was observed throughout the PDZ core that is suggestive of an overall small increase in backbone dynamics in p^{397}-PDZ3. These results are similar to that found in Δ7ct, which showed large increases in side-chain dynamics and subtle increases in backbone dynamics (21). From the ^{15}N relaxation analysis, it is also noteworthy that protein tumbling was significantly retarded by the unfolding of α3 as indicated by the increased global tumbling correlation time, τ_m, which increased from 5.9 to 6.8 ns upon phosphorylation at Tyr-397. This tumbling time is also consistent with an increased volume for the PDZ3 core (to be reported elsewhere).[3]

Phosphorylation Disrupts PDZ3-SH3 Association—In vivo, phosphorylation does not occur in the specific PDZ construct used here (residues 304–402), but rather, it occurs in the context of full-length PSD-95 (Fig. 1*A*). Although it may not be feasible to probe this 80-kDa protein for phosphorylation effects by NMR, we hypothesized that some full-length behavior might be captured in shorter multidomain constructs. Thus, we set out to characterize the behavior of PDZ3 in a construct that spans residues 304–532, which includes the SH3 domain and the linker preceding it. In addition, the F-strand from the GK domain (residue numbers 713–724) was added to the C terminus to enhance stability (16). This PDZ3-SH3 construct yielded reasonable quality HSQC spectra (supplemental Fig. S4) from which the effects of phosphorylation could be monitored.

In PDZ3 alone, phosphorylation at Tyr-397 initiated α3 undocking and a redistribution of its sampled conformations. In the intact MAGUK, because α3 precedes a ~25-residue linker that connects to the SH3, phosphorylation may affect putative domain packing between PDZ3 and SH3. To test this, ^{15}N backbone transverse relaxation times (T_2) were measured in PDZ3-SH3. T_2 times are highly sensitive to the rate of tumbling experienced by individual sites. An overall increase in T_2 is expected for a reduced degree of domain-domain packing because loss of packing would lead to more time spent tumbling as an isolated domain. For these experiments, phosphorylation at 397 in PDZ3-SH3 was mimicked by the Y397E mutation, which yielded a ~7-fold reduction in CRIPT binding affinity in the context of the PDZ3 construct (supplemental Fig. S5). The validity of the mimic was also confirmed by $^{13}C^{\alpha}$ chemical shifts. These shifts indicate an almost identical loss of helicity (relative to unphosphorylated PDZ3) in Y397E-PDZ3 compared with p^{397}-PDZ3 (Fig. 5).

T_2 values for the mutant and wild-type constructs were measured, and their differences are shown in Fig. 7*A*. In general, Y397E-PDZ3-SH3 showed T_2 values that are ~3–25 ms longer relative to wild type. The increase in T_2 at virtually all residues suggests that phosphorylation at Tyr-397 reduced the interaction between PDZ3 and SH3, which appeared to be stabilized by the presence of α3 helical secondary structure.

Two additional serine phosphorylation sites (Ser-415 and Ser-418) within the PDZ3-SH3 linker region have been reported (42). The fragment where Ser-415 and Ser-418 are located corresponds to a fragment that was shown to contribute to communication between PDZ3 and GK in the PSD-95 homologue Dlg-1 (25). Specifically, deletion or replacement of this "Δ2" fragment with random coil segments (from Gly-Ser repeats) abolishes the PDZ3-depdendent interaction of the GK domain with GukHolder. Because of the proximity of these res-

[3] C. M. Petit, A. B. Law, P. J. Sapienza, J. Zhang, X. Zuo, and A. L. Lee, manuscript in preparation.

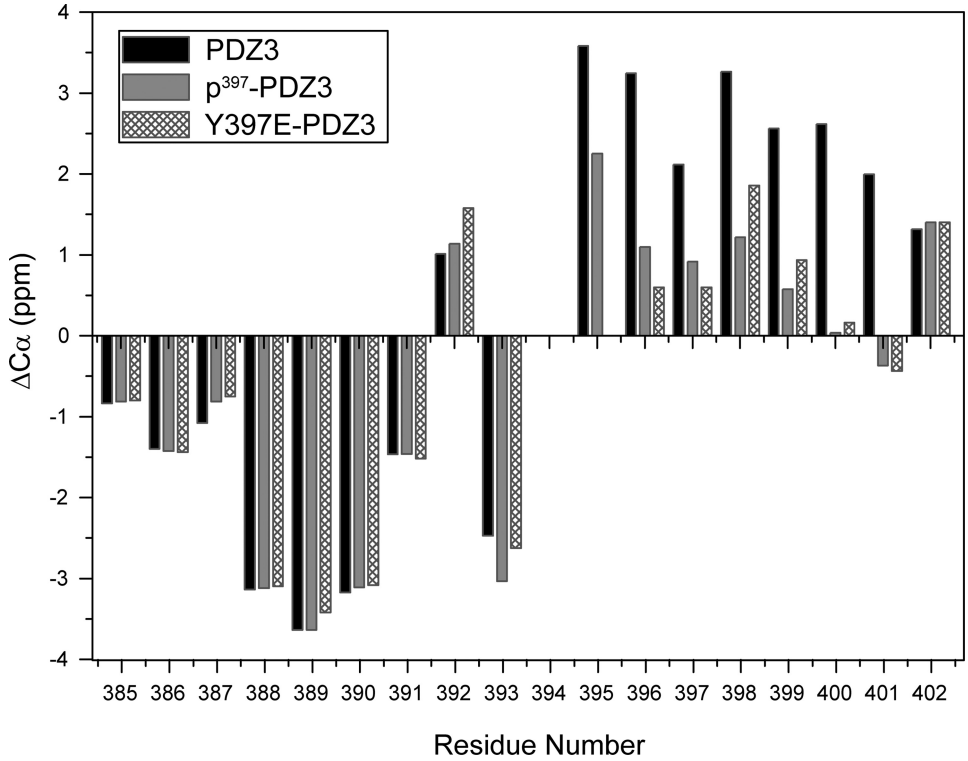

FIGURE 5. **C^{α} chemical shift differences of PDZ3, p^{397}-PDZ3, and Y397E-PDZ3 relative to random coil values.** The C^{α} chemical shift differences were calculated by subtraction of random coil C^{α} chemical shifts from those of PDZ3, p^{397}-PDZ3, or Y397E-PDZ3. Only β5 and α3 are shown for clarity. The random coil chemical shifts were used as reported by Wishart and Sykes (40).

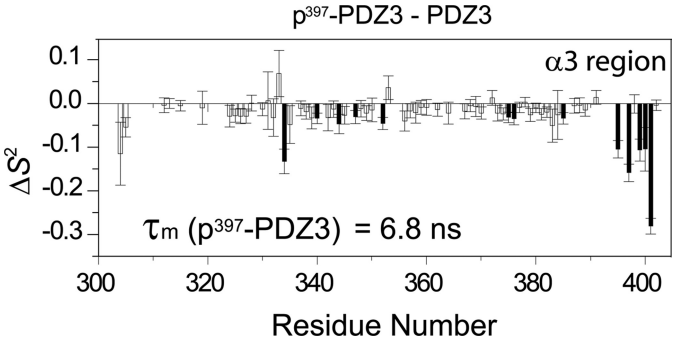

FIGURE 6. **Backbone amide order parameters (S^2).** The ΔS^2 was calculated by subtraction of unphosphorylated PDZ3 S^2 from p^{397}-PDZ3 S^2 values. The residues with significant order parameter changes ($\Delta S^2 > 2\sigma$) are shown as *filled bars*. Data were acquired at 500 MHz. *Error bar*, S.D.

idues to α3 and their conserved nature (Fig. 1*B*), we created a triple phosphorylation mutant to test the effect of phosphorylation at these two additional sites. ^{15}N T_2 measurements were made on a Y397E/S415E/S418E triple mutant of PDZ3-SH3. Compared with the Y397E single mutant, the triple mutant exhibited even higher T_2 values (Fig. 7*B*), suggesting stronger dissociation of PDZ3 and SH3 domains.

DISCUSSION

Regulation in PDZ Domains—When PDZ domains are excised from their parent proteins, they typically behave as simple binders of C termini, which is documented by the many determined structures of individual PDZs and their cognate ligands (43). Current evidence indicates, however, that PDZ function can be influenced by flanking sequences and/or domains as well as intermolecular interactions (30). For example, the PDZ domain of Par6 alters its binding affinity for ligand upon binding of Cdc42 to the semi-Crib motif, which is immediately N-terminal to the PDZ domain, and augments its β-sheet (18). In a reverse sense, "PDZ proteases" are regulated by ligand-induced changes in PDZ structure (20). PDZ function has also been shown to be regulated by redox events within the PDZ domain (44), and this redox potential can be allosterically regulated by binding to yet another PDZ domain (45). The idea that PDZ domains are involved in higher order regulatory events is consistent with their locations (often in tandem) in proteins involved in organization of signaling complexes, subcellular transport, and cell-cell adhesion (9, 43).

Here, we show how PDZ3 from PSD-95 is regulated by phosphorylation of Tyr-397, which lies outside the strict PDZ boundary in a C-terminal extension that augments the PDZ core structure (14, 21). Although phosphorylation was shown to regulate function of the PDZ protein NHERF1, the phosphorylation sites are far from the PDZ domains, and their precise mechanism of release of autoinhibition remains to be elucidated (26). In contrast to phosphorylation of PDZ domains themselves, there are numerous examples of phosphorylation of PDZ substrates (46–54). Phosphorylation typically occurs at positions −2 to −4, and although this usually results in weakening of the PDZ-ligand interaction, there are examples of phosphorylation strengthening the interaction (49, 53, 54). Thus, phosphorylation appears to be a recurring regulatory mechanism in PDZ-mediated interactions. Although there is currently little direct characterization of how phosphorylation influences PDZ domains, proteomics work suggests that phos-

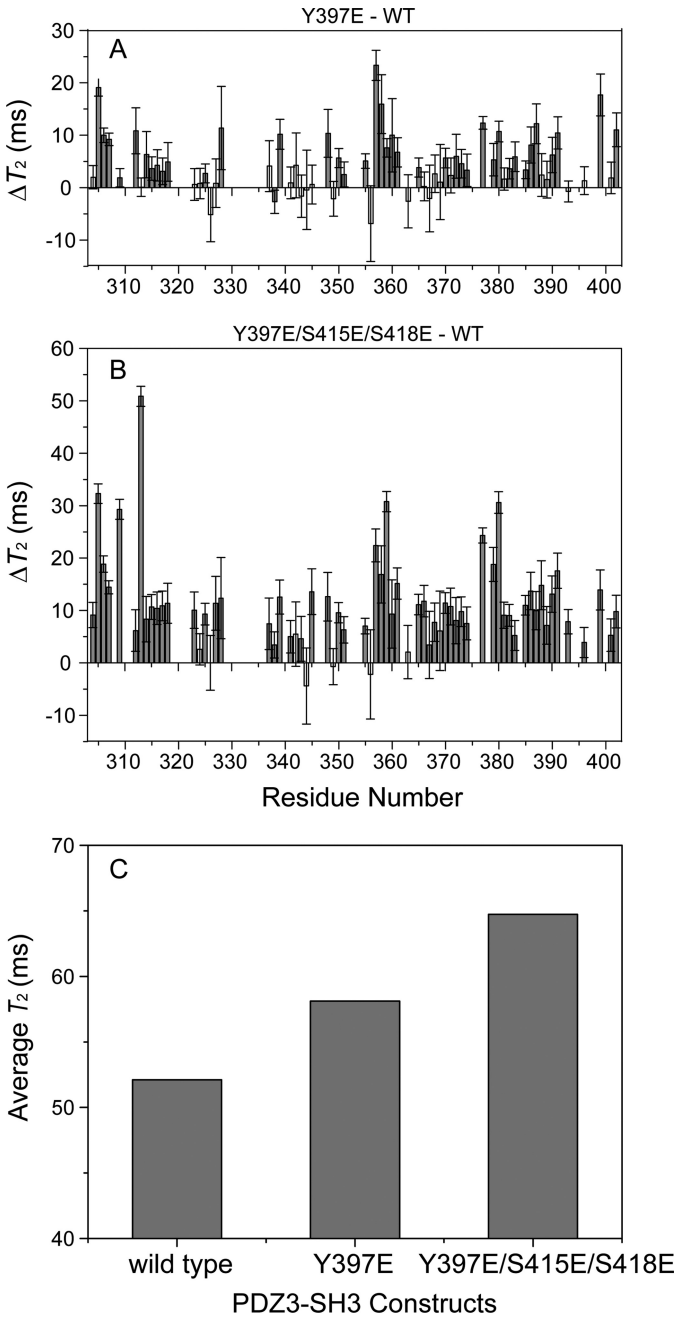

FIGURE 7. **T_2 analysis of PDZ3-SH3 wild type and Y397E and Y397E/S415E/S418E mutants.** *A*, T_2 difference between Y397E-PDZ3-SH3 single mutant and wild-type PDZ3-SH3. *B*, T_2 difference between PDZ3-SH3 Y397E/S415E/S418E triple mutant and wild-type PDZ3-SH3. *C*, the average T_2 values for wild type and single and triple mutants. In *A* and *B*, residues with significant T_2 increases are shown as *filled bars*. *Error bar*, S.D.

phorylation in PDZ core or flanking sequences is relatively common. As collected in the UniProt database, numerous phosphorylation sites have been experimentally confirmed (mostly in murine proteins) for the PDZ proteins ZO-1, GRIP1, MAGI2, MAGI3, and Par3, for example. Many of these phosphorylation sites exist in short linkers between domains as observed here in PSD-95 but also within the PDZ domains.

Phosphorylation at Tyr-397 Allosterically Regulates Binding of C Terminus—We successfully phosphorylated (at Tyr-397) a construct of PDZ3 that includes an α-helical C-terminal extension that ends at position 402. A combination of chemical shift analysis, amide hydrogen exchange, and ^{15}N relaxation showed that phosphorylation partially undocks the α3 helix from the PDZ3 core. The linear change in chemical shifts (Fig. 4) indicates that p^{397}-PDZ3 exists as a rapid equilibrium between a docked state in which α3 is natively packed and an undocked state in which "α3 residues" have lost some helical character. This conclusion was only possible because of previous characterization of Δ7ct, which eliminates the native α3 by truncation of residues 396–402 (21). In that study, α3 was shown to confer a 21-fold increase in binding affinity to CRIPT peptide. Without α3, the PDZ3 core has enhanced side-chain dynamics that are quenched upon CRIPT binding. This confers an entropic penalty to binding, which was detected through isothermal titration calorimetry. Interestingly, because α3 does not contact CRIPT peptide, this was considered a novel dynamic allosteric mechanism. Here, we show that this dynamic mechanism has biological significance and was induced by phosphorylation at Tyr-397. The 4-fold reduction in CRIPT binding affinity (as opposed to 21-fold) is consistent with the ~50% population of undocked α3. The behavior of p^{397}-PDZ3 also confirmed that Δ7ct serves as an excellent proxy for phosphorylated PDZ3 constructs.

Phosphorylation Tunes Interdomain Interactions in PDZ3-SH3-GK MAGUK Core—A caveat of the results on p^{397}-PDZ3 (residues 304–402) here is that the construct remains artificial as an excised domain. (One reason in support of using this construct is that phosphorylation at Tyr-397 was less efficient upon further extension of the C terminus and hence yields of such phosphorylated constructs were unacceptably low.) Nevertheless, the role of the linker may be important. Although there is no crystal structure of full-length PSD-95 or the PDZ-SH3-GK supradomain from any MAGUK, there is evidence for interaction between PDZ3 and SH3-GK. From electron microscopy, intact PSD-95 appears as a "C-shaped" arrangement of domains (55). In other work, binding assays on various constructs of PSD-95 family MAGUKs suggest interdomain allostery between PDZ3 and the SH3-GK module. In the case of PSD-95, PDZ3 (as well as PDZs 1 and 2) was shown to influence binding of MAP1a, which binds to the GK domain (24). A similar result was found for SAP97 (a closely related PSD-95 family MAGUK) binding to guanylate-kinase-associated protein (56). In the case of the PSD-95 homologue Dlg-1 from *Drosophila*, PDZ3 influences binding of GukHolder, which binds to the SH3 domain (25). Structural insight into how PDZ3 and its following linker interact with SH3-GK is needed to unravel the basis for these interactions and how they are regulated.

To gain insight into how PDZ3 interacts with SH3-GK and whether phosphorylation plays a role, we studied a PDZ3-linker-SH3 construct. ^{15}N T_2 measurements within the PDZ3 domain for wild type as well as for a Y397E phosphomimic and a triple phosphomimic construct, Y397E/S415E/S418E, were made. Ser-415 and Ser-418 have also been confirmed to be phosphorylated (28, 29), and therefore a combination of these sites may be phosphorylated under different signaling and cell contexts. Phosphorylation at Tyr-397 increased the mobility of PDZ3, and this effect was increased further for the triple mutant (Fig. 7). This is consistent with a model in which PDZ3

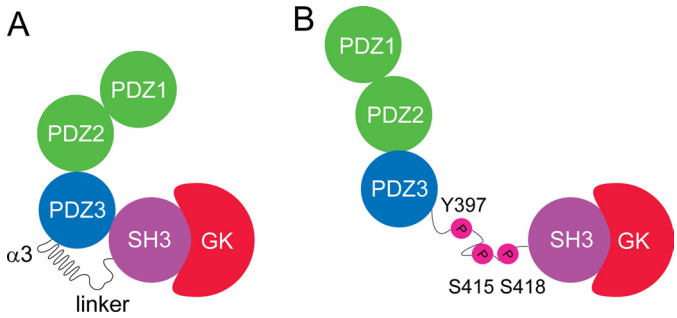

FIGURE 8. **Schematic of phosphorylation at Tyr-397, Ser-415, and Ser-418 in PSD-95.** The third α-helix in PDZ3 is undocked upon phosphorylation, which consequently interrupts the domain packing between PDZ3 and SH3.

interacts with SH3-GK via the SH3 domain and phosphorylation at 397 in α3 and 415/418 in the linker disrupts this interaction (Fig. 8). To our knowledge, these are the first reported physical data that relate PDZ3 to SH3 for any MAGUK. To date, there are no reported structures for any construct containing PDZ3 and SH3 domains, although structural models of PDZ3-SH3-GK have been proposed (56, 57). The T_2 results suggest that additive phosphorylation interferes with the putative PDZ3-SH3 interaction. Because positions 415 and 418 are well beyond the PDZ3 domain (and extension), the T_2 data also suggest that the linker plays a role in the association of PDZ3 and SH3. It is currently unknown whether phosphorylation at these sites occur in an ordered pattern, but it is possible that phosphorylation of Ser-415/Ser-418, which are seated in a putatively flexible fragment (SSLGSG), precedes phosphorylation of Tyr-397, which is mostly buried. Phosphorylation of Ser-415/Ser-418 may then facilitate Tyr-397 phosphorylation by loosening the domain packing between PDZ3 and SH3 or providing binding sites for the kinase that phosphorylates Tyr-397. Overall, our NMR relaxation measurements suggest that phosphorylations of Tyr-397, Ser-415, and Ser-418 cooperate together to regulate interdomain communication of PSD-95.

It is currently unclear how conserved these phosphorylation events are. The PSD-95 family of proteins comprises PSD-95, PSD-93, SAP97, and SAP102. Although there is high sequence conservation in the α3 and linker among these proteins, phosphorylation at Tyr-397 has only been confirmed for PSD-95 and PSD-93, and phosphorylation at 415/418 has only been observed so far in PSD-95. Although it may be possible that differences in phosphorylation patterns in this region contribute to functional differences between these MAGUKs (which also have functional redundancies), this cannot be resolved until more in-depth phosphorylation mapping is carried out.

Concluding Remarks—PDZ domains are primarily appreciated for their simple function of binding C-terminal sequences. However, PDZs are typically embedded in lengthy protein sequences characterized by multiple other structured domains and significant stretches of unknown structure/flexibility. Understanding native PDZ function therefore often requires consideration of these additional elements. There are now a number of examples of PDZ domains whose core structures are augmented by N- or C-terminal extensions (14, 22, 58–60), and a recent review predicts that one-third of PDZ domains contain such structural augmentations (30). We show here that the effects of such additional segments can be dynamically modulated by phosphorylation, building upon previous work that showed that the external segments can regulate PDZ function. In many multidomain proteins, the role of interdomain linkers is not well understood. By mimicking phosphorylation at Tyr-397 and in the linker of the PDZ3-linker-SH3 construct from PSD-95, progressive increases in mobility in PDZ3 due to linker phosphorylation were detected. This suggests that the linker plays a key role in supradomain assembly. We propose that linkers in MAGUKs and in other PDZ proteins can adopt varying degrees of structure/flexibility that serve to tune interdomain communication.

Acknowledgments—We thank Jennifer Cable (Department of Biochemistry and Biophysics, University of North Carolina at Chapel Hill (UNC-CH)), Karl Koshlap (NMR Facility, Eshelman School of Pharmacy, UNC-CH), Ashutosh Tripathy (Macromolecular Interactions Facility, UNC-CH), Yanbao Yu (Department of Biochemistry and Biophysics, UNC-CH), Dan Cline (Eshelman School of Pharmacy, UNC-CH), and Brenda Temple (Structural Bioinformatics Facility, UNC-CH) for technical assistance. We also thank John Kuriyan for providing the expression plasmid for Src kinase.

REFERENCES

1. Sprang, S. R., Acharya, K. R., Goldsmith, E. J., Stuart, D. I., Varvill, K., Fletterick, R. J., Madsen, N. B., and Johnson, L. N. (1988) *Nature* **336,** 215–221
2. Huse, M., and Kuriyan, J. (2002) *Cell* **109,** 275–282
3. Aghazadeh, B., Lowry, W. E., Huang, X. Y., and Rosen, M. K. (2000) *Cell* **102,** 625–633
4. Pufall, M. A., Lee, G. M., Nelson, M. L., Kang, H. S., Velyvis, A., Kay, L. E., McIntosh, L. P., and Graves, B. J. (2005) *Science* **309,** 142–145
5. Lee, C. W., Ferreon, J. C., Ferreon, A. C., Arai, M., and Wright, P. E. (2010) *Proc. Natl. Acad. Sci. U.S.A.* **107,** 19290–19295
6. Pawson, T., Gish, G. D., and Nash, P. (2001) *Trends Cell Biol.* **11,** 504–511
7. Good, M. C., Zalatan, J. G., and Lim, W. A. (2011) *Science* **332,** 680–686
8. Funke, L., Dakoji, S., and Bredt, D. S. (2005) *Annu. Rev. Biochem.* **74,** 219–245
9. Sheng, M., and Hoogenraad, C. C. (2007) *Annu. Rev. Biochem.* **76,** 823–847
10. Anderson, J. M. (1996) *Curr. Biol.* **6,** 382–384
11. Gardoni, F., Marcello, E., and Di Luca, M. (2009) *Neuroscience* **158,** 324–333
12. Xu, W. (2011) *Curr. Opin. Neurobiol.* **21,** 306–312
13. Kim, E., and Sheng, M. (2004) *Nat. Rev. Neurosci.* **5,** 771–781
14. Doyle, D. A., Lee, A., Lewis, J., Kim, E., Sheng, M., and MacKinnon, R. (1996) *Cell* **85,** 1067–1076
15. Long, J. F., Tochio, H., Wang, P., Fan, J. S., Sala, C., Niethammer, M., Sheng, M., and Zhang, M. (2003) *J. Mol. Biol.* **327,** 203–214
16. McGee, A. W., Dakoji, S. R., Olsen, O., Bredt, D. S., Lim, W. A., and Prehoda, K. E. (2001) *Mol. Cell* **8,** 1291–1301
17. Tavares, G. A., Panepucci, E. H., and Brunger, A. T. (2001) *Mol. Cell* **8,** 1313–1325
18. Peterson, F. C., Penkert, R. R., Volkman, B. F., and Prehoda, K. E. (2004) *Mol. Cell* **13,** 665–676
19. Yan, J., Pan, L., Chen, X., Wu, L., and Zhang, M. (2010) *Proc. Natl. Acad. Sci. U.S.A.* **107,** 4040–4045
20. Sohn, J., Grant, R. A., and Sauer, R. T. (2007) *Cell* **131,** 572–583
21. Petit, C. M., Zhang, J., Sapienza, P. J., Fuentes, E. J., and Lee, A. L. (2009) *Proc. Natl. Acad. Sci. U.S.A.* **106,** 18249–18254
22. Bhattacharya, S., Dai, Z., Li, J., Baxter, S., Callaway, D. J., Cowburn, D., and Bu, Z. (2010) *J. Biol. Chem.* **285,** 9981–9994
23. LaLonde, D. P., Garbett, D., and Bretscher, A. (2010) *Mol. Biol. Cell* **21,**

1519–1529
24. Brenman, J. E., Topinka, J. R., Cooper, E. C., McGee, A. W., Rosen, J., Milroy, T., Ralston, H. J., and Bredt, D. S. (1998) *J. Neurosci.* **18,** 8805–8813
25. Qian, Y., and Prehoda, K. E. (2006) *J. Biol. Chem.* **281,** 35757–35763
26. Li, J., Poulikakos, P. I., Dai, Z., Testa, J. R., Callaway, D. J., and Bu, Z. (2007) *J. Biol. Chem.* **282,** 27086–27099
27. Ballif, B. A., Carey, G. R., Sunyaev, S. R., and Gygi, S. P. (2008) *J. Proteome Res.* **7,** 311–318
28. Trinidad, J. C., Specht, C. G., Thalhammer, A., Schoepfer, R., and Burlingame, A. L. (2006) *Mol. Cell. Proteomics* **5,** 914–922
29. Munton, R. P., Tweedie-Cullen, R., Livingstone-Zatchej, M., Weinandy, F., Waidelich, M., Longo, D., Gehrig, P., Potthast, F., Rutishauser, D., Gerrits, B., Panse, C., Schlapbach, R., and Mansuy, I. M. (2007) *Mol. Cell. Proteomics* **6,** 283–293
30. Wang, C. K., Pan, L., Chen, J., and Zhang, M. (2010) *Protein Cell* **1,** 737–751
31. An, Y., Ji, J., Wu, W., Lv, A., Huang, R., and Wei, Y. (2005) *Appl. Microbiol. Biotechnol.* **68,** 774–778
32. Bradshaw, J. M., and Waksman, G. (1998) *Biochemistry* **37,** 15400–15407
33. Seeliger, M. A., Young, M., Henderson, M. N., Pellicena, P., King, D. S., Falick, A. M., and Kuriyan, J. (2005) *Protein Sci.* **14,** 3135–3139
34. Muhandiram, D. R., and Kay, L. E. (1994) *J. Magn. Reson. B* **103,** 203–216
35. Fuentes, E. J., Der, C. J., and Lee, A. L. (2004) *J. Mol. Biol.* **335,** 1105–1115
36. Lin, D., Sze, K. H., Cui, Y., and Zhu, G. (2002) *J. Biomol. NMR* **23,** 317–322
37. Kalia, L. V., and Salter, M. W. (2003) *Neuropharmacology* **45,** 720–728
38. Xue, Y., Ren, J., Gao, X., Jin, C., Wen, L., and Yao, X. (2008) *Mol. Cell. Proteomics* **7,** 1598–1608
39. Palmer, A. G., 3rd, Kroenke, C. D., and Loria, J. P. (2001) *Methods Enzymol.* **339,** 204–238
40. Wishart, D. S., and Sykes, B. D. (1994) *J. Biomol. NMR* **4,** 171–180
41. Sapienza, P. J., and Lee, A. L. (2010) *Curr. Opin. Pharmacol.* **10,** 723–730
42. Collins, M. O., Yu, L., Coba, M. P., Husi, H., Campuzano, I., Blackstock, W. P., Choudhary, J. S., and Grant, S. G. (2005) *J. Biol. Chem.* **280,** 5972–5982
43. Zhang, M., and Wang, W. (2003) *Acc. Chem. Res.* **36,** 530–538
44. Mishra, P., Socolich, M., Wall, M. A., Graves, J., Wang, Z., and Ranganathan, R. (2007) *Cell* **131,** 80–92
45. Liu, W., Wen, W., Wei, Z., Yu, J., Ye, F., Liu, C. H., Hardie, R. C., and Zhang, M. (2011) *Cell* **145,** 1088–1101
46. Cao, T. T., Deacon, H. W., Reczek, D., Bretscher, A., and von Zastrow, M. (1999) *Nature* **401,** 286–290
47. Chung, H. J., Huang, Y. H., Lau, L. F., and Huganir, R. L. (2004) *J. Neurosci.* **24,** 10248–10259
48. Chung, H. J., Xia, J., Scannevin, R. H., Zhang, X., and Huganir, R. L. (2000) *J. Neurosci.* **20,** 7258–7267
49. Hegedüs, T., Sessler, T., Scott, R., Thelin, W., Bakos, E., Váradi, A., Szabó, K., Homolya, L., Milgram, S. L., and Sarkadi, B. (2003) *Biochem. Biophys. Res. Commun.* **302,** 454–461
50. Massari, S., Vanoni, C., Longhi, R., Rosa, P., and Pietrini, G. (2005) *J. Biol. Chem.* **280,** 7388–7397
51. Parker, L. L., Backstrom, J. R., Sanders-Bush, E., and Shieh, B. H. (2003) *J. Biol. Chem.* **278,** 21576–21583
52. Popovic, M., Bella, J., Zlatev, V., Hodnik, V., Anderluh, G., Barlow, P. N., Pintar, A., and Pongor, S. (2011) *J. Mol. Recognit.* **24,** 245–253
53. Stein, E. L., and Chetkovich, D. M. (2010) *J. Neurochem.* **113,** 42–53
54. Tyler, R. C., Peterson, F. C., and Volkman, B. F. (2010) *Biochemistry* **49,** 951–957
55. Nakagawa, T., Futai, K., Lashuel, H. A., Lo, I., Okamoto, K., Walz, T., Hayashi, Y., and Sheng, M. (2004) *Neuron* **44,** 453–467
56. Wu, H., Reissner, C., Kuhlendahl, S., Coblentz, B., Reuver, S., Kindler, S., Gundelfinger, E. D., and Garner, C. C. (2000) *EMBO J.* **19,** 5740–5751
57. Korkin, D., Davis, F. P., Alber, F., Luong, T., Shen, M. Y., Lucic, V., Kennedy, M. B., and Sali, A. (2006) *PLoS Comput. Biol.* **2,** e153
58. Hillier, B. J., Christopherson, K. S., Prehoda, K. E., Bredt, D. S., and Lim, W. A. (1999) *Science* **284,** 812–815
59. Krojer, T., Garrido-Franco, M., Huber, R., Ehrmann, M., and Clausen, T. (2002) *Nature* **416,** 455–459
60. Pan, L., Yan, J., Wu, L., and Zhang, M. (2009) *Proc. Natl. Acad. Sci. U.S.A.* **106,** 5575–5580